Pereira JM, Rosseti F, Lourenço PB (2021) Numerical modelling of grouted anchors in masonry walls. International Journal of Masonry Research and Innovation – Special issue: Simple Mechanical Models for Unreinforced Historic Masonry Constructions, 7(2): 32-60.
https://www.inderscienceonline.com/doi/abs/10.1504/IJMRI.2022.119876

# Numerical modelling of grouted anchors in masonry walls

**Keywords:** Masonry, grouted anchors, numerical modelling, finite element method

**Abstract:** This work aims to numerically simulate experimental pull-out tests in masonry wall anchors. Advanced Finite Element (FE) 3D models were built to fully reproduce the loadbearing capacity, the failure mode, the stresses and the force-displacement curve and, in general, all the phenomena involved for both brick and stone specimens. Three different modelling approaches were considered. First, a macro-model was adopted, where both brick and stone masonry were assumed as a homogeneous isotropic material. The steel bar and the grouted mortar of the anchor system were considered linear elastic and the system was placed in the specimen using interfaces. The second approach was a unit model, developed with the aim to reproduce the influence of the unit where the anchoring fastening is located. The last approach studied was a micro-model, where both the units and the mortar are considered. The challenge in modelling these systems is highlighted from the different modelling strategies used and compared.

Pereira JM, Rosseti F, Lourenço PB (2021) Numerical modelling of grouted anchors in masonry walls. International Journal of Masonry Research and Innovation – Special issue: Simple Mechanical Models for Unreinforced Historic Masonry Constructions, 7(2): 32-60.
https://www.inderscienceonline.com/doi/abs/10.1504/IJMRI.2022.119876

## 1. Introduction

Masonry buildings are known to be vulnerable to earthquakes, particularly if inadequately tied together. They are generally able to support vertical loads, but they lack capacity to withstand large horizontal loads. Unreinforced masonry buildings are, generally, constituted by several walls organised in orthogonal planes and their seismic vulnerability is a result of their mass, which then produces high forces of inertia. Considering that these structures have very low tensile strength, this often results in brittle failure and consequently sudden collapse (Torrealva, 2012).

Masonry constructions have different types of failure modes when subjected to seismic events. These failure modes depend on factors such as, the geometry of the building, the mechanical properties of the mortar and unit (Varum et al, 2014), or the stiffness of the floors (Betti et al, 2014; Scotta et al 2018). Two different types of failure can be highlighted: a) in-plane failure (diagonal tension, toe crushing, rocking and sliding); b) out-of-plane failure (flexural hinge lines) (Lourenço et al, 2011; Tolles et al, 1996) (Figure 1). Usually, out-of-plane failure is the most critical failure mode.

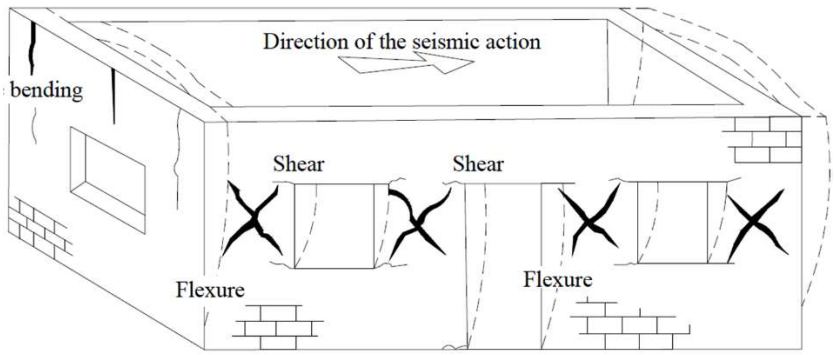


*Figure 1 – Typical damage to structural walls (adapted from Tomasevic (1990)).*

The interaction between in-plane and out-of-plane walls, as well as the diaphragms – through connections – has considerable influence in the seismic response of a masonry

building (Betti et al, 2014; Scotta et al 2018). A good connection between vertical elements (walls) and horizontal elements (floors) leads to what is called "*box behaviour*" of the buildings. When box behaviour is achieved, the response of the structure to horizontal loads is improved (Lourenço et al, 2011). The structural global performance of traditional buildings under seismic actions depends on the possibility to redistribute the horizontal loads within the vertical elements (Lourenço et al, 2011). For this reason, the connections between the different parts of the structure play a key role. In fact, the improvement of the connections between the different elements of the structure became the most important issue in the recent years (Lourenço et al, 2018).

In the specific case of ancient masonry buildings, where specific issues must be considered (minimum intervention, quality requirements, aesthetics and compatibility with the features of the building, intervention costs and facility of the procedures), anchors seem to be particularly well suited (Lourenço et al, 2018; Torrealva and Vicente 2014; Blondet et al, 2006). Other strengthening solutions, aimed at reducing the deficiency of connections, are available such as reinforced plastered walls using meshes made of steel, polymers or other materials (Lourenço et al, 2018; Torrealva and Vicente 2014; Blondet et al, 2006).

Usually, anchors are divided according to their type, as: *Grouted anchors, Adhesive anchors and Mechanical anchors* (Cook, 2006). Most of the available literature on anchoring system focuses in concrete substrates (Cook, 2006; Banholzer et al, 2005; Benmokrane et al, 2000; Dudeka and Kadela, 2016; Wang et al, 2017), and just a few authors deal with the specific case of masonry (Muñoz et al, 2019; Muñoz and Lourenço, 2019; Moreira et al, 2014; Gigla, 2004). However, the general considerations are similar for both materials.

The present work focuses on grouted anchors applied on masonry substrate. According to experimental studies, the weakest component of an anchoring system in masonry seems to be the masonry itself, considering its low tensile and shear strength, rather than the steel or the grout interfaces (Banholzer et al, 2005; Benmokrane et al, 2000). There are two different interfaces when considering grouted anchors. These interfaces are responsible for the load transfer between the masonry and the steel element: a) the inner interface – grout/steel element; b) the outer interface – grout/masonry. This type of anchoring system can be classified in four different failure mechanism (Araújo, 2014) (Figure 2): a) failure of the steel: the applied load is able to reach the steel's yielding strength (Figure 2a); b) failure of the masonry: a failure surface similar to a cone is formed in the masonry surrounding the anchor (Figure 2b); c) failure at the interface grout/masonry (outer interface) (Figure 2c); d) failure at the interface grout/steel (inner interface) (Figure 2d).

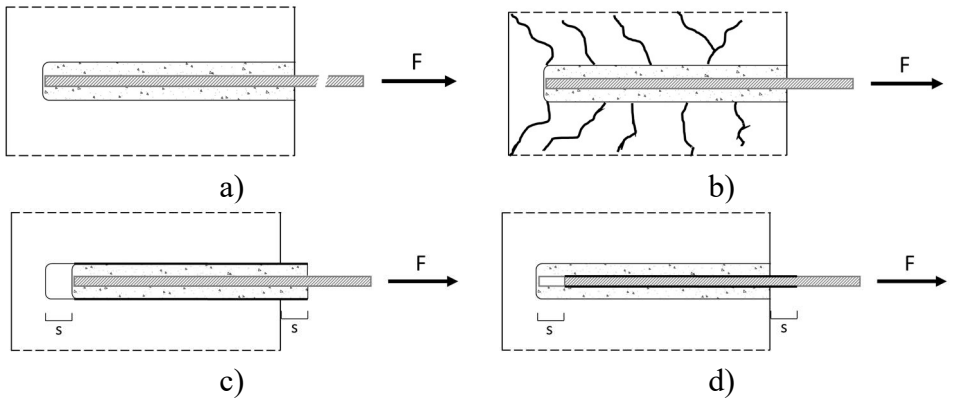


*Figure 2 - Failure mechanisms in anchoring systems: (a) Failure of the steel; (b) Failure of the masonry; (c) Failure at the interface grout/masonry; (d) Failure at the interface grout/steel (adapted from Araújo, 2014)*

This work presents numerical modelling strategies dealing with the application of grouted anchors in different types of masonry walls. Here, the objective is to highlight the challenges in modelling this type of structural system, focusing on grouted anchors with

failure occurring on the masonry (masonry cone failure). The numerical models, using different approaches are calibrated and compared with experimental results. The obtained results are presented, compared and analysed. With the obtained results, concluding remarks are drawn.

Besides this introduction, the present work is comprised of three other sections. Section 2 presents the experimental work that was conducted previously and is used to compare the different numerical models. Section 3 includes the considerations taken to build the numerical models, the initial material properties calibration, the assumptions regarding the modelling of the anchor and the different modelling strategies used. Section 4 gathers the main conclusions observed throughout this work, focusing on the different models used to replicate the experimental behaviour of these grouted anchors.

## 2. Experimental pull-out tests

This work intends to model experimental tests, performed at University of Minho (Portugal), of grouted anchors in both stone (Muñoz et al, 2019) and brick (Muñoz and Lourenço, 2019) masonry walls. Besides the information presented below, additional details regarding the experimental campaigns can be found in (Muñoz et al, 2019) and (Muñoz and Lourenço, 2019) for stone and brick masonry walls, respectively.

The grouted anchor, used in the tests was composed of a steel bar and an injection grout, applied according to the manufacturer recommendations (Muñoz et al, 2019; Muñoz and Lourenço, 2019). As stated, two different masonry panels were tested, using the same test setup and the same lime mortar, together with high strength granite stone units (Muñoz et al, 2019) and low strength clay bricks (Muñoz and Lourenço, 2019).

Figure 3a shows the geometry of the specimens. A pre-compression (vertical load) of 0.2 MPa was applied in all tests. The setup configuration of the test allowed applying the vertical load to the masonry in an initial phase, which was then maintained during the test. Six LVDTs (Linear Variable Displacement Transducer) were used to monitor displacements (on the anchor, on the anchor's stone, inside the masonry failure cone, and outside of the masonry failure cone) (Muñoz et al, 2019; Muñoz and Lourenço, 2019) (Figure 3b). Each specimen was bound to the loading setup using a steel square frame that prevented overturning of the panel subjected to the pull-out force. The experiment was carried out using displacement control and a displacement rate of 0.003 mm/s (Muñoz et al, 2019; Muñoz and Lourenço, 2019).

This work focuses on the modelling of grouted anchors in which failure occurred at the masonry (Figure 2b). From the available experimental tests, two typical tests were considered, one for brick masonry (Figure 4a) and one for stone masonry (Figure 4b). The obtained maximum capacities were 20.78 kN and 28.95 kN for the brick and stone masonry, respectively. The failure mode of these two walls was by cone failure of the masonry (Figure 5).

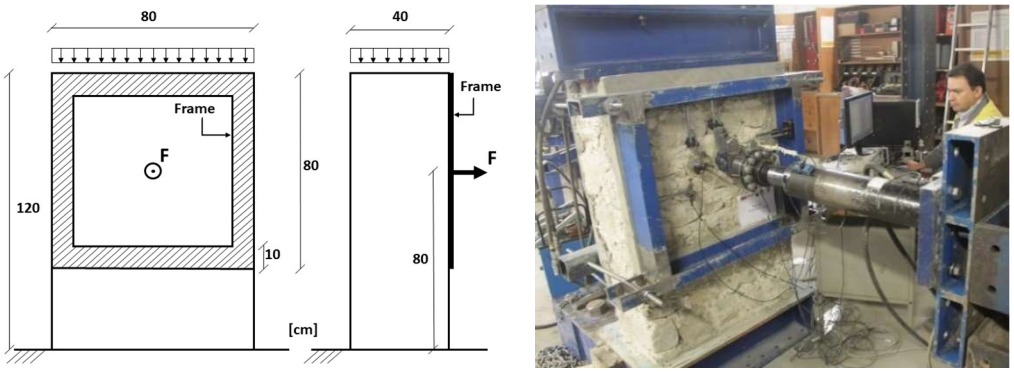


*Figure 3 - Experimental setup (Muñoz et al, 2019): a) Geometry of the specimens [cm]; b) Pull-out test*

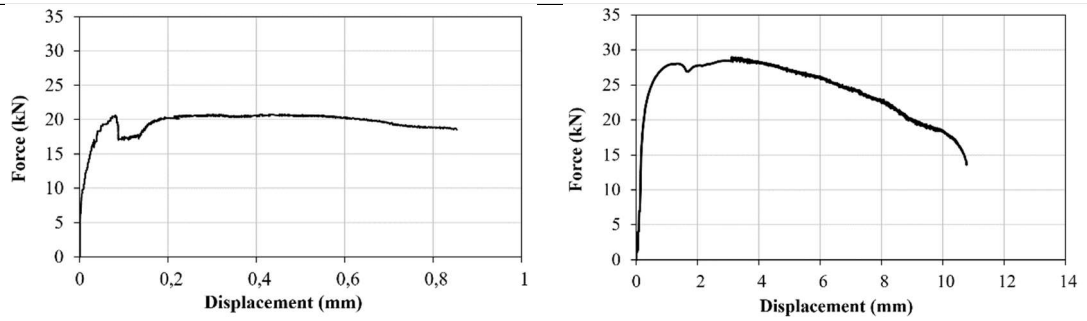


a) b)

*Figure 4 - Force-displacement curves for the pull-out tests: a) brick masonry (Muñoz and Lourenço, 2019); b) stone masonry (Muñoz et al, 2019)*

a) b)

*Figure 5 - Pull-out experimental failure mode: a) brick masonry (Muñoz and Lourenço, 2019); b) stone masonry (Muñoz et al, 2019)*

## 3. Numerical modelling

In order to reproduce the behaviour observed in the experimental pull-out tests, different numerical modelling strategies were developed. All the analyses were performed using the Finite Element Method with the software DIANA 10 (Manie and Kikstra, 2016) The models were developed using different modelling approaches. In this section, all the numerical models are presented, as well as their main results.

The numerical models adopted the real geometry of the specimens and the experimental setup (Figure 3a). Specific geometrical considerations regarding the different modelling approaches are discussed in the section pertaining to the numerical approach. For each

step of the non-linear analyses, the equilibrium is achieved with a regular Newton-Raphson iterative method and an internal energy-based convergence criterion with a tolerance of $10^{-3}$ (Manie and Kikstra, 2016). The constitutive models, used to describe the behaviour of the materials, are described in the next sections.

### 3.1. Masonry

A Total Strain Rotating Crack (TSRC) material model that is available in DIANA (Manie and Kikstra, 2016) was used to model the non-linear behaviour of the masonry, and it is usually adequate for this purpose (Pereira et al, 2020; Aşıkoğlu et al, 2020; Ciocci et al, 2018). This material model describes the stress as a function of the strain and follows a smeared approach for the fracture energy. The crack direction rotates with the principal strain axes, ensuring that the crack remains normal to the direction of the maximum principal strain, and the shear softening occurs implicitly as a result of the principal stress and strain conditions. The cracking phenomenon for the TSRC constitutive law is quantified by the integral under the stress–strain diagram, denoted as fracture energy $G_f^I$ for tension and $G_c$ for compression (Figure 6). In Figure 6, $f_c$ and $f_t$ stands for the compressive and tensile strength of masonry whereas $h$ corresponds to the crack bandwidth, which in this case was regularized to ensure mesh independency. Parabolic behaviour for compression (Figure 6a) and exponential behaviour for tension (Figure 6b) were used to describe the post-peak behaviour of the masonry (Manie and Kikstra, 2016).

In order to use these constitutive models, it is necessary to define a set of parameters related to the mechanical properties of the material. From the experimental campaigns, it was possible to obtain the average compressive strength for both brick and stone masonry, being 9.84 MPa and 1.81 MPa, respectively (Muñoz et al, 2019; Muñoz and Lourenço,

2019). The compressive fracture energy was obtained multiplying the compressive strength by a ductility index ($d = 1.6$ mm, for $f_c < 12$ MPa) (Lourenço, 2009). The Young's Modulus ($E$) and the tensile properties ($f_t$ and $G^I_f$) were obtained by calibrating simple and homogenised numerical models of diagonal compression tests conducted on walls built with the same materials (Figure 7).

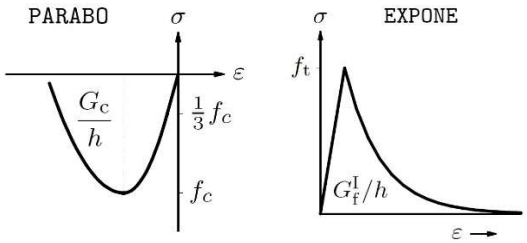


*Figure 6 – Masonry Constitutive model: a) Parabolic compressive softening; b) Exponential tensile softening (Manie and Kikstra, 2016)*

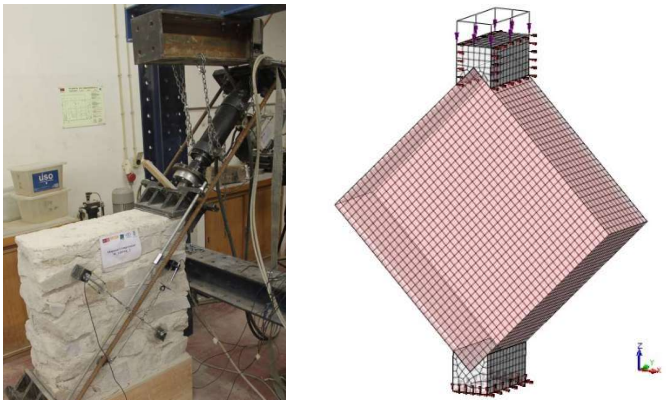


*Figure 7 – Masonry mechanical properties: a) diagonal compression tests (Muñoz et al, 2019); b) numerical model for diagonal compression tests*

The mechanical properties that produced the best fit in terms of numerical results can be seen in Table 1. The comparison between the experimental and numerical results can be seen in Figure 8a for the brick wall and Figure 8b for the stone wall. Here, the direction of analysis is the direction of the load, and the positive displacements are downwards. As

can be seen from the results, the maximum capacity is well estimated, and the obtained values are within what is available in the literature (NTC, 2018).

*Table 1 – Masonry non-linear mechanical properties*

| Property | Brick masonry | Stone masonry |
|---|---|---|
| Young's modulus, $E$ (GPa) | 1.5 | 1.0 |
| Poisson's ratio, $v$ (-) | 0.20 | 0.20 |
| Compressive strength, $f_c$ (MPa) | 9.84 | 1.81 |
| Fracture energy in compression, $G_c$ (N/mm) | 16.0 | 3.00 |
| Tensile strength, $f_t$ (MPa) | 0.08 | 0.06 |
| Mode-I Fracture energy, $G_f$ (N/mm) | 0.01 | 0.015 |

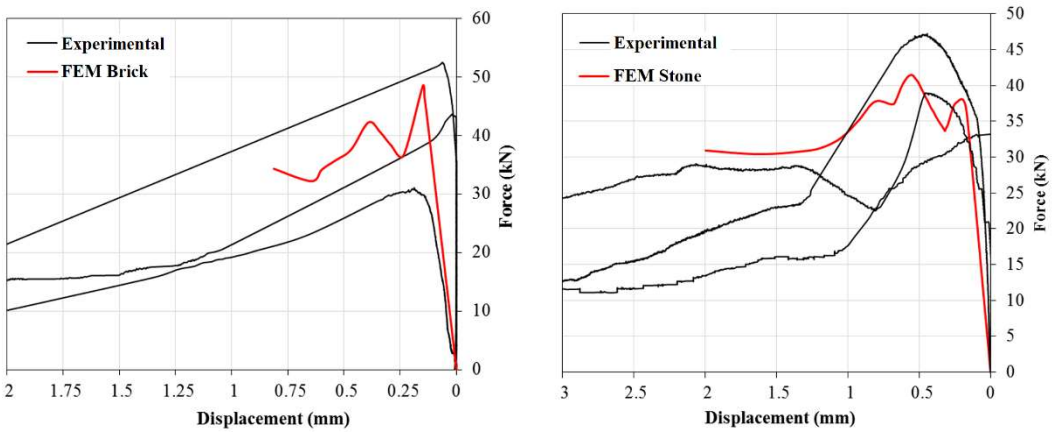


a) b)

*Figure 8 – Force-displacement curves for both experimental and numerical diagonal compression tests: a) Brick wall; b) stone wall.*

## 3.2. Anchor system

The anchor and the grout were modelled as a cylindrical solid, respectively with 19 cm of length and 1 cm of diameter for the steel bar, and 15 cm of length and 2 cm of diameter for the mortar (Figure 9). These were positioned in the centre of the masonry, even if in the real test they were located in the centre of the area delimitated by the external frame. This simplification does not have any influence on the test behaviour, since even in the experimental case the bar is far from the external support and is not affected by the

boundary condition. The role of the frame is, in fact, to prevent the overturning of the entire specimen due to the pull-out load application.

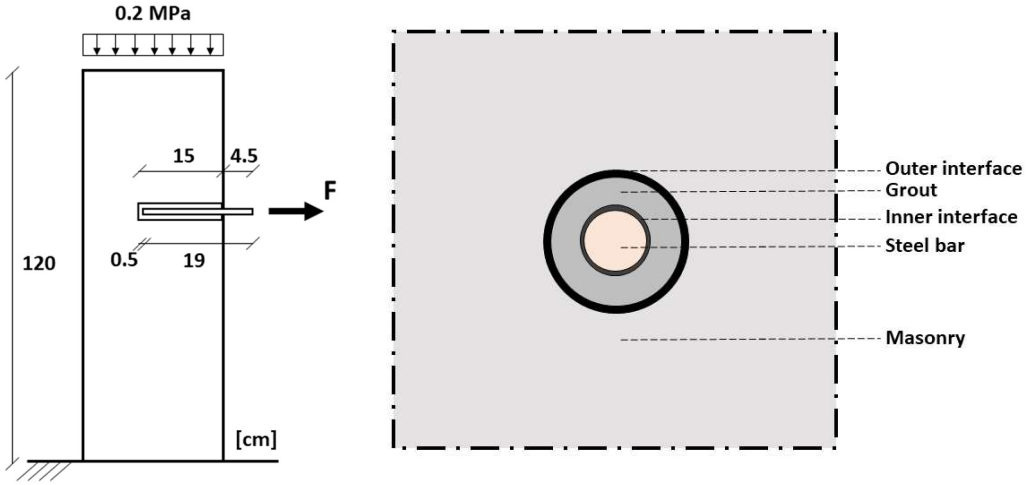


*Figure 9 – Pull-out test model: a) geometry and position of the anchor; b) modelling strategy for the anchor system (adapted from Araújo, 2014)*

The bond between grout/masonry (outer) and grout/steel (inner) was modelled using interface elements. These are capable of describing the relation between the normal stresses, shear stresses and displacements across the surface (Manie and Kikstra, 2016). The interface's elastic behaviour is defined with a normal and tangential stiffness. The experimental characterization of the bond of the two previously presented interfaces was not carried out. As such, the available literature was used to define the interface stiffness (Gigla, 2004; Araújo, 2014). The particular set of values adopted is in accordance to the work presented by (Araújo, 2014) (Table 2). It is noticed that the elastic stiffness $k$ of the $z$ and $y$ directions indicate the normal stiffness. Since their limited influence, in particular for what concerned the maximum resistance (Araújo, 2014), these values were kept equal in all analyses performed. After the experimental tests, the specimens were carefully inspected. This inspection allowed to conclude that it is reasonable to assume that the

behaviour of the interfaces is linear, as there was no damage in the grout of the tested specimens (Muñoz et al, 2019). For the steel elements, standard values were used, $E$ = 210 GPa and $v$ = 0.3. For the cementitious grout, the manufacturer's information was used, $E$ = 27 GPa and $v$ = 0.2.

*Table 2 – Values used for the numerical interfaces.*

| Property | Outer interface | Inner interface |
|---|---|---|
| Stiffness $k_X$ (N/mm$^3$) | 100 | 200 |
| Stiffness $k_Y$ (N/mm$^3$) | 100 | 200 |
| Stiffness $k_Z$ (N/mm$^3$) | 50 | 100 |

The mesh is composed of isoparametric solid brick elements of eight nodes and tetrahedral elements of five nodes, HX24L and PY15L (Manie and Kikstra, 2016), for the masonry and grout materials. The three-dimensional interface elements have eight and six nodes, Q24IF and T18IF (Manie and Kikstra, 2016), (Figure 10). The mesh size was a compromise between efficiency and accuracy.

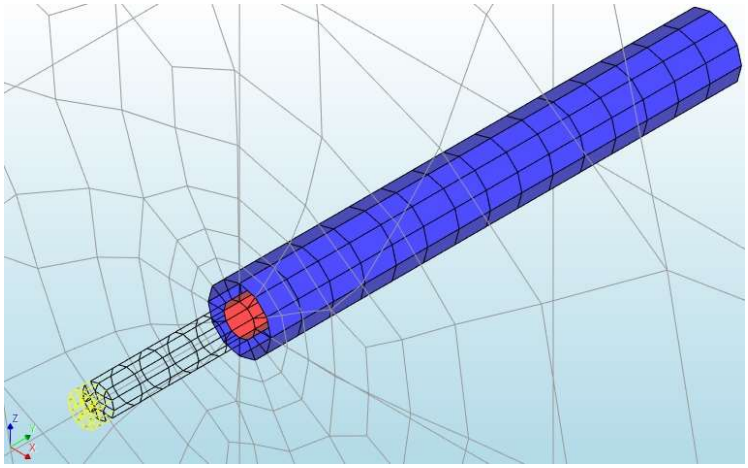

*Figure 10 – Inner numerical interface (red) and outer grout/masonry interface (blue one).*

### 3.3. Numerical results

Different modelling strategies are possible when dealing with masonry structures (Lourenço, 1996) (Figure 11): a) Detailed micro-model, where the mortar and the unit are modelled as continuum elements and the interface between mortar and unit is modelled as a discontinuum element; b) Simplified micro-model, where the units (expanded) are modelled as continuum elements while the mortar and the interface mortar/unit is modelled together with discontinuum elements; and c) macro-model, where all the materials are idealized as a continuum.

Three different modelling approaches were pursued in this work with the intention to reproduce and discuss the experimental results obtained in section 2, using FE models: a) macro-model; b) unit model; and c) micro-model. The macro-model considers the masonry as a homogeneous and isotropic material. The unit model also considers the masonry as a homogeneous and isotropic material, with a special unit placed in the anchor system, according to the observed results. The micro-model considers both the unit and the mortar within the wall. In the next section the results obtained with the different modelling approaches are discussed.

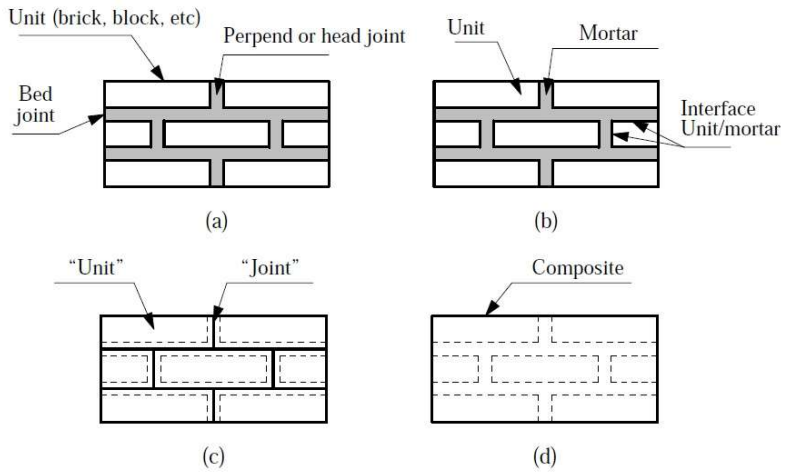


*Figure 11 – Different strategies for modelling masonry: (a) masonry sample; (b) detailed micro- model; (c) simplified micro-model; (d) macro-model (Lourenço, 1996)*

### 3.3.1. Macro-model

The first modelling approach assumes masonry as a composite material (Lourenço, 1996; Lourenço, 2009). Several authors have been using this modelling strategy for masonry obtaining adequate responses (Berto et al, 2004; Betti and Vignoli, 2008; Abruzzese et al, 2009; Annecchiarico et al, 2009). An advantage of using this modelling strategy is the reduced computational time when compared with micro-model, which usually required denser and complex finite element meshes (Lourenço, 2002).

Two different models were developed considering this approach: a) brick masonry; and b) stone masonry. In this modelling approach, the only difference between both models is the masonry mechanical properties (Table 1). The FE mesh is composed of 2784 nodes and 4010 elements. Here, the mesh was refined in the anchor system and its surrounding area, where higher stress variations are expected. The regions where the stress variation is expected to be smooth have a less refined mess. For the steel anchor and for the cementitious mortar, mesh elements with a maximum of 10 mm were used, while for the masonry a mesh maximum dimension equal to 100 mm was set. The mesh homogenization was then automatically done by the software. The final mesh can be seen in Figure 12.

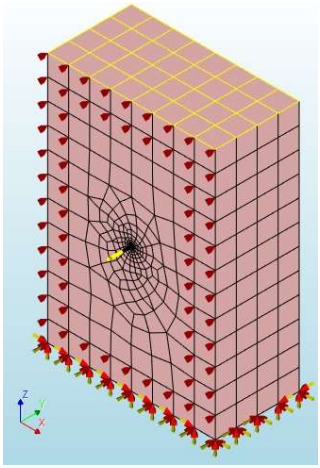

*Figure 12 – Macro-model for the pull-out tests*

Using the mechanical properties reported in section 3.1, the obtained results, in terms of force – displacement curves can be seen in Figure 13 for brick and stone masonry. When comparing both numerical and experimental curves, it is possible to observe a significant difference in both the peak force and the linear behaviour. The maximum capacity obtained numerically is 8.87 kN (20.78 kN for experimental, with 57% difference) and 7.20 kN (28.95 kN for experimental, with 75% difference) for the brick and stone masonry, respectively. It is evident that the model provides a value of loadbearing capacity too conservative, when compared to the experimental one. This value is indicative of an incorrect modelling approach.

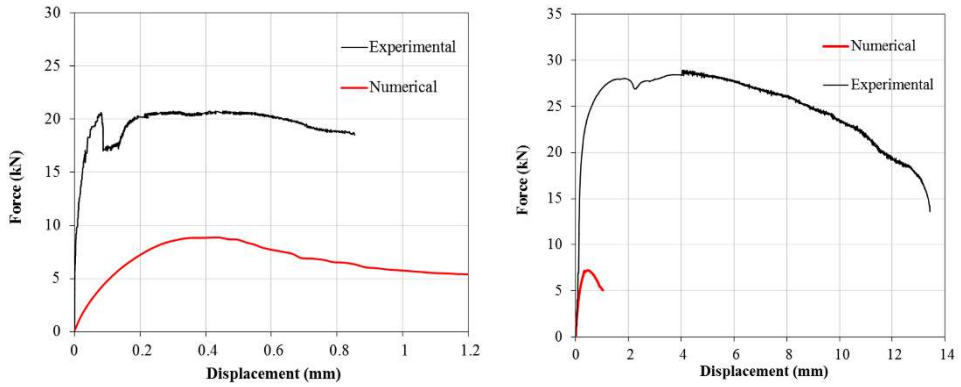


*Figure 13 – Numerical versus experimental curves: a) brick masonry wall; b) stone masonry wall.*

Considering the failure mode (Figure 14), both models were able to properly reproduce the masonry cone failure (Figure 5). It is noticed that the masonry cone does not include all the thickness of the wall, but its propagation affects the material until about the middle of the section. Until the peak stage, the cone is symmetrical with reference to the horizontal axis of the steel anchor. After that, the development of the cone is somewhat less symmetrical due the adopted mesh.

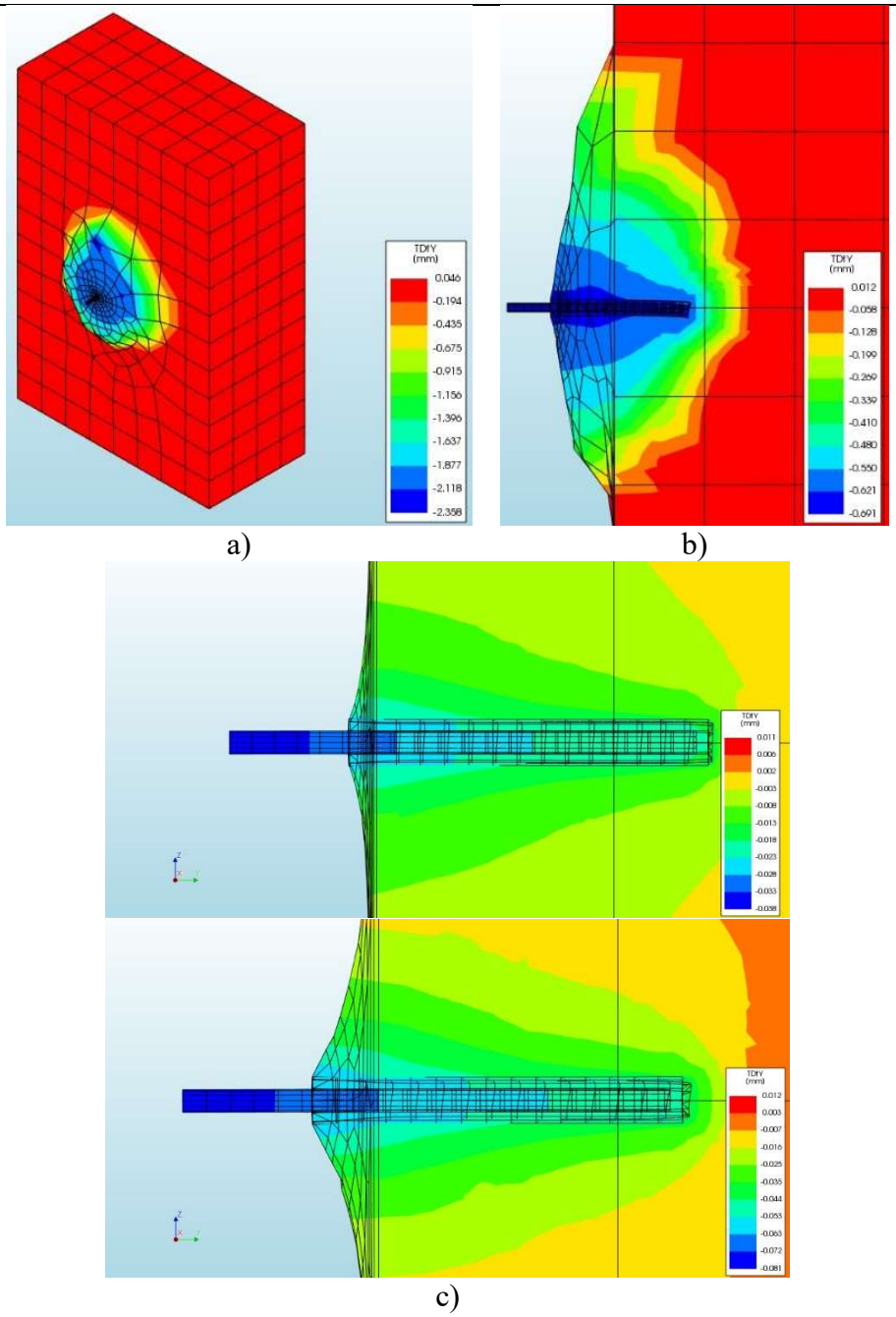


*Figure 14 – Deformed mesh for the numerical model: a) isoparametric view; b) side view; c) linear deformation of the interfaces during initial load application.*

The obtained results with this modelling approach are far from replicating the experimental curves. This is due to the nature of the problem at hand. This anchor system, when applied this type of masonry wall, produces a local failure mechanism rather than a global one. It should also be highlighted that the anchor and the grout are normally

arranged in a single unit of the wall (brick or stone) (Muñoz et al, 2019). This means that using averaged mechanical properties from diagonal compressive tests, does not seem to be a reasonable option, leading to a clear underestimation of the anchor capacity.

With the objective of obtaining a better fit of the numerical results, another analysis was made with the macro-models. This time, the mechanical properties (for both brick and stone masonry) were changed according to the considerations described next. Table 3 presents the new properties as well as the properties obtained from the diagonal compression tests, for comparison, with the valued changed highlighted in grey. With this new set of mechanical properties, the obtained results, in terms of force – displacement curves can be seen in Figure 15. Here, the maximum capacity obtained is 20.90 kN (20.78 kN for experimental, with 0.57% difference) and 27.00 kN (28.95 kN for experimental, with 6.7% difference) for the brick and stone masonry, respectively.

*Table 3 – Masonry non-linear material properties for both diagonal compression and pull-out tests*

| Property | Brick masonry | | Stone masonry | |
|---|---|---|---|---|
| | Diagonal compression tests | Pull-out tests | Diagonal compression tests | Pull-out tests |
| Young's modulus, $E$ (GPa) | 1.5 | 2.0 | 1.0 | 1.0 |
| Poisson's ratio, $v$ (-) | 0.20 | 0.20 | 0.20 | 0.20 |
| Compressive strength, $f_c$ (MPa) | 9.84 | 9.84 | 1.81 | 9.50 |
| Fracture energy in compression, $G_c$ (N/mm) | 16.0 | 16.0 | 3.0 | 15.2 |
| Tensile strength, $f_t$ (MPa) | 0.08 | 0.50 | 0.06 | 0.95 |
| Mode-I Fracture energy, $G_f$ (N/mm) | 0.01 | 0.02 | 0.015 | 0.05 |

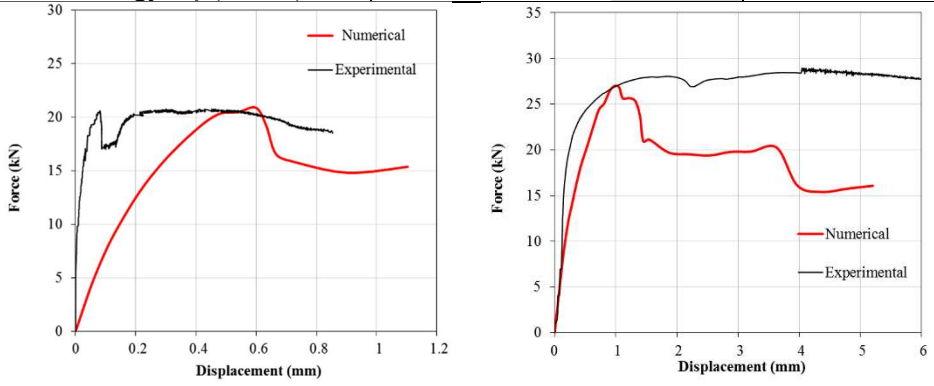


*Figure 15 – Numerical versus experimental curves using the new set of mechanical properties: a) for the brick masonry wall; b) for the stone masonry wall*

Regarding the new materials properties for the brick masonry wall, the compressive part was kept the same; the Young's modulus was increased to 2000 MPa, a value higher than the one extracted from the diagonal compression tests, but still in the literature's acceptable range (NTC, 2018). The tensile fracture energy was set to 0.02 N/mm, a value double of the previous one, but still acceptable (Lourenço, 2009), and the tensile strength was increased to 0.5 MPa, more than 5 times the previous value. Because, as stated previously, the anchor and the grout are normally arranged in a unit of the wall, the resistance depends on local mechanisms of stress transmission, on the position of the anchor and, most of all, on the unit characteristics. To consider this phenomenon, the tensile strength of this material was increased making an average of the tensile strength of the mortar (very low value, near zero) and the one of the brick unit (2.13 MPa obtained by experimental characterization (Muñoz et al, 2019)). With this new set of parameters, the numerical curve is able to properly replicate the maximum capacity of the anchor for the brick wall, despite the difference in the initial stiffness. As expected, the tensile properties of the material are the ones with the most influence the results.

Regarding the new material properties for the stone masonry wall, the pull-out behaviour is deeply influence by the characteristics of the stone where the anchor is located. Taking this into consideration, a new approach was used to assess the mechanical properties of the wall. The compressive and the tensile strength of the stone masonry were estimated from the mechanical characteristics of its components. The compressive strength of the macro-model was estimated as the sum of the percentage of stone volume inside the specimen multiplied by its compressive strength value and the percentage of mortar volume multiplied by its compressive strength:

$$f_c = \%\, V_{stone} \times f_{c,stone} + \%\, V_{mortar} \times f_{c,mortar} \quad (1)$$

For this analysis, the mechanical values obtained experimentally, for stone and mortar, were considered: $f_{c,stone}$ = 28.74 MPa and $f_{c,mortar}$ = 1.63 MPa (Muñoz et al, 2019). The estimation of the value of stone and mortar was obtained using a graphical procedure. Both the front face and the side face of the wall were analysed and averaged (Figure 16). Here, the procedure was to use photographs of the wall and measure the stone to mortar ratio. Figure 16 shows an example of the measurements performed in both direction of the wall. From the analysis of the images, it was possible to obtain the percentage of stone and mortar on the surface of the wall, being 57.6% and 42.4%, respectively. Using Eq. (1), a compressive strength of 17.25 MPa is obtained. Because only the surface is being analysed and the distribution of units inside the wall could be different, it was decided to decrease this value by 45%. Setting the compressive strength as 9.5 MPa (55% of 17.25 MPa). The tensile strength was taken as one tenth of the compressive strength, being 0.95 MPa, which is usually assumed by other authors for homogeneous materials (Lourenço, 2009). The tensile fracture energy was increased to 0.05 N/mm to consider the reciprocally ductile relation. It is a high value but still inside to the literature's range (Lourenço, 2009).

It is clear, from the results presented in this section, that the macro-modelling approach is able to reproduce the maximum capacity of pull-out tests in both brick and stone masonry. However, limitations have been identified, being the most important the fact that in the case of pull-out tests, the unit in which the anchor is applied is of paramount importance, being brick or stone. This can be seen in the experimental tests, however, the numerical models based on the macro-modelling approach require additional considerations to take this adequately into account.

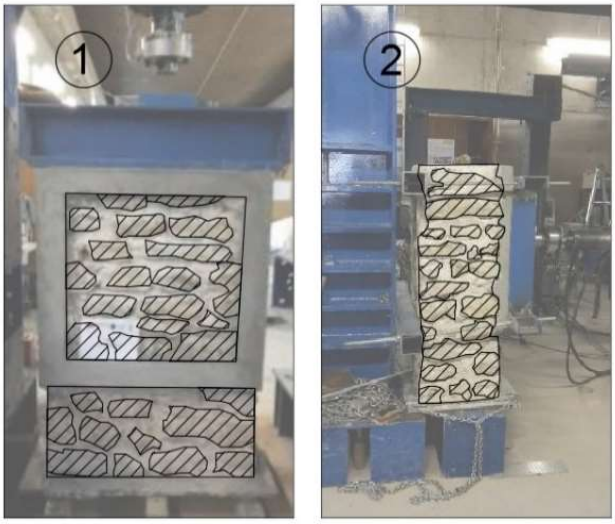


*Figure 16 – Graphical estimation of the percentage of constituents' volume (57.6% stone and 42.4% mortar)*

### 3.3.2. Unit model

This type of model is an evolution of the macro-model approach used in the previous section. Its purpose is to try to consider the fact that the anchor and the grout are normally arranged in a single unit of the wall. The modelling approach was suitably developed to try and fully reproduce the damage evolution observed in the experimental tests. In fact, the cone failure could mobilize an entire unit, a half-unit or a bigger surface in correspondence of the mortar's layer. This is more pronounced for the stone masonry, however, models for both the brick and stone masonry walls were developed. The analysis of the damage pattern for the experimental test, has revealed that the cone failure occurs without the rupture of the stone where the anchor is inserted (Muñoz et al, 2019).

The considerable dimension of the unit, which could be compared with the dimension of the specimen, affects in a large extent the test results. The unit model, here presented is unique, since in the literature nothing similar was found. It derives from the observation that the dimensions and the mechanical properties of the unit where the system anchor-grout is inserted locally affects the masonry behaviour. This leads to a simple model,

where the unit is modelled as a linear elastic solid and it is positioned inside the masonry, which is defined as a macro nonlinear element.

The geometry of the unit model, regarding the general features, is the same of the macro-model studied above. The only difference is the elastic unit, which was designed approximating the shape and the volume of the central unit with an equivalent solid prism (Figure 17). This element was placed in the middle of the frame area without using any interface element. In such a way, the unit is prevented to slide along the pull-out force direction. Both boundary conditions and loads were kept the same as in the macro-model. The unit was defined as a linear elastic material and the material's inputs are reported in Table 4, according to their experimental characterization (Muñoz et al, 2019; Muñoz and Lourenço, 2019). Its mesh was defined with a maximum size of 25 mm per element, while for the rest of the mesh the same dimensions as before were used (Figure 18).

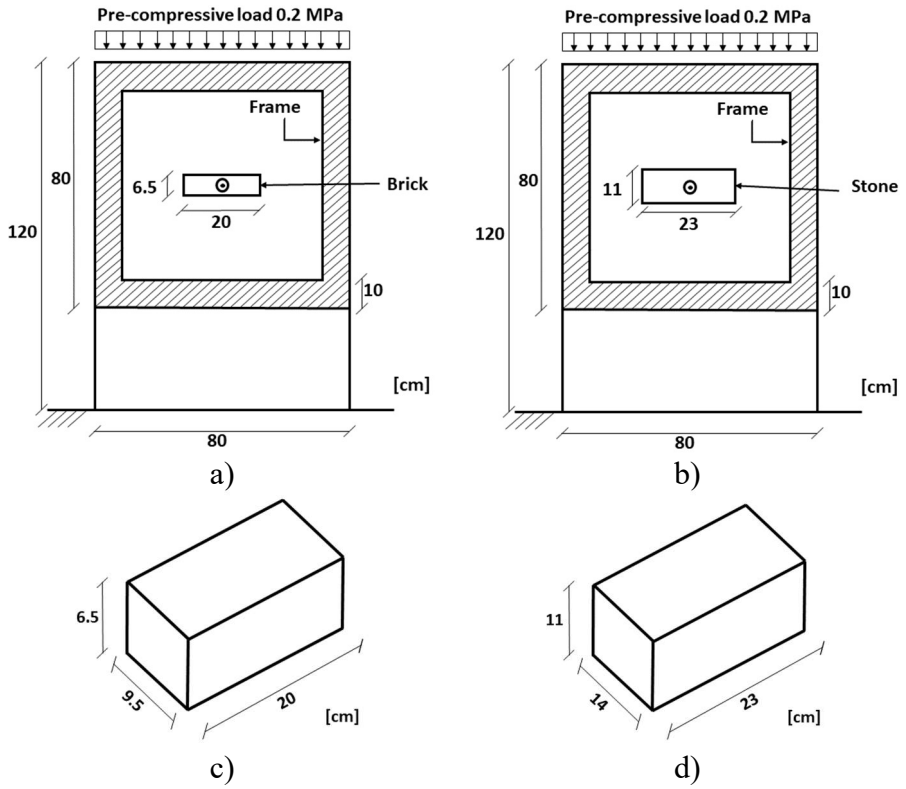


*Figure 17 – Unit model: a) schematic of the brick masonry model; b) schematic of the stone masonry model; c) brick unit; d) stone unit*

*Table 4 – Unit elastic properties for the unit model (Muñoz et al, 2019; Muñoz and Lourenço, 2019)*

| Property | Brick unit | Stone unit |
|---|---|---|
| Young's modulus, $E$ (GPa) | 9.74 | 58.7 |
| Poison ratio, $v$ | 0.20 | 0.20 |

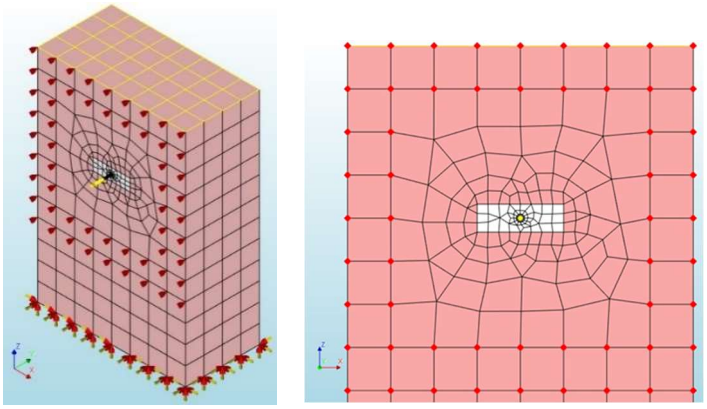

a) b)

*Figure 18 – Unit model: a) global mesh of the FE model; b) detail of the unit's mesh*

The objective of this model is to use the mechanical properties derived from the diagonal compression tests (Table 1) and, by including this unit in the anchor application area, to reach results closer to the ones obtained experimentally (Figure 4). The obtained results, in terms of force – displacement curves, can be seen in Figure 19 for both masonry walls. These results should be compared with the ones obtained by the full macro-model with the mechanical properties derived from the diagonal compression tests (Figure 13). The numerical curve moved towards the experimental one. In term of the brick wall, the increase of the maximum capacity was modest (26% increase, compared with macro-model, Figure 13a). However, for the stone wall, the increase of the maximum capacity was considerable (163% compared with macro-model, Figure 13b). This phenomenon is more pronounced in the stone masonry wall. Compared with the experimental results, the capacity is still underestimated, however, with much less difference than the full macro-

model. Here, the maximum capacity obtained is 11.21 kN (20.78 kN for experimental, with 46% difference) and 19.0 kN (28.95 kN for experimental, with 34% difference) for the brick and stone masonry, respectively. The failure modes are also quite similar to those reported in the experimental tests and the full macro-model.

Similar to the macro-model (Section 3.3.1) it would be possible to obtain a better fitting between the numerical curve and the experimental curve for the unit model, by changing the mechanical parameters introduced in the numerical analyses. However, the purpose of the model was to check the possibility of obtaining better results with, mostly, a macro-modelling approach, but without having to go through all the consideration used in the previous section to obtain valid results with a macro-modelling approach.

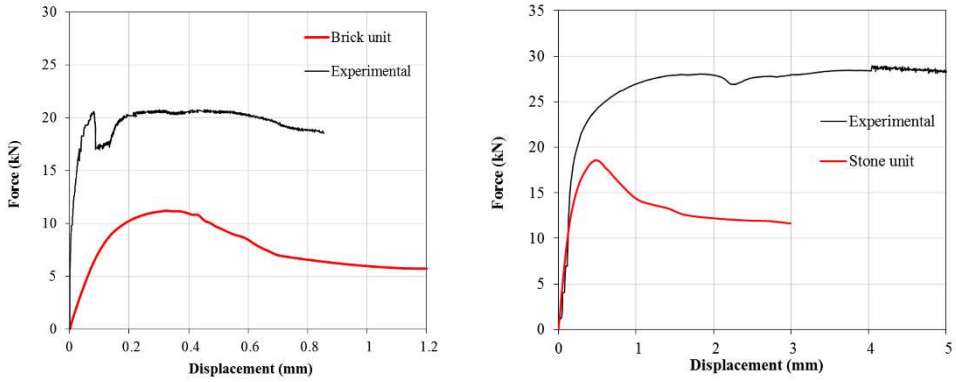


a) b)

*Figure 19 – Numerical (unit model) versus experimental curves: a) brick masonry wall; b) stone masonry wall.*

### 3.3.3. Micro-model

Finally, the micro-model approach was performed to evaluate if a more detailed model would provide better results, regarding the maximum capacity, the total displacement and the failure mode. In this case, only the brick masonry wall was modelled, since it has a regular geometry. Each brick was separately modelled according to the wall texture, linked by mortar layers. The first operation was to define the wall geometry, in particular

each horizontal course. The final geometric configuration used for the micro-model can be seen in Figure 20.

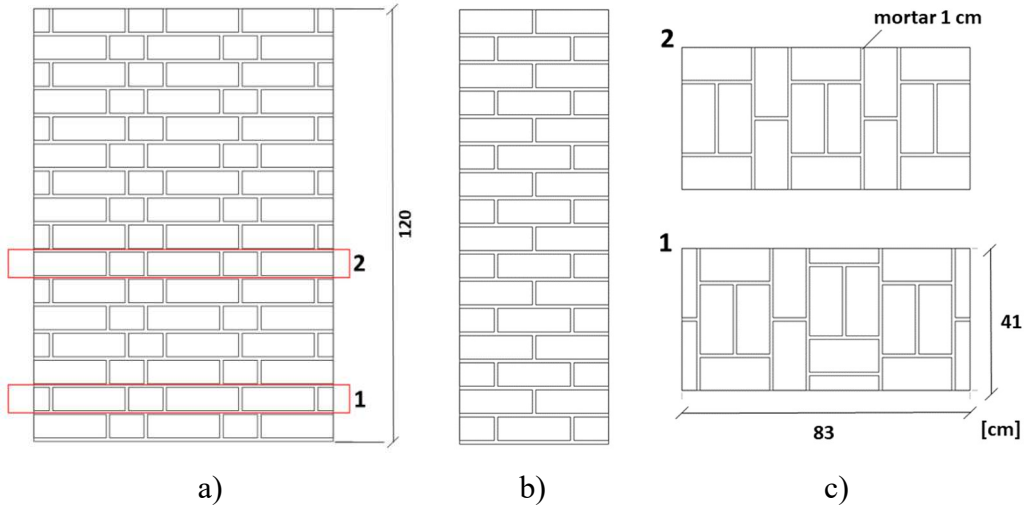


a) b) c)

*Figure 20 – Brick wall geometric configuration used for the micro-model [cm]: a) front view; b) side view; c) horizontal courses details*

The model was developed without interfaces between units and mortar for simplicity. In such a way sliding is prevented, but this is expected not to affect the pull-out final result, extensively. The same boundary conditions and loads were applied to the model, as discussed in the previous sections. Regarding the mesh dimension for each element, it was decided to use 10 mm for steel and grout, 25mm for the bricks near the anchor, 40 mm for the normal bricks and for the mortar layers, 120 mm for the bricks located far from the steel bar (Figure 21). The final FE mesh is composed of 19272 nodes and 33648 elements.

The mechanical properties used in the micro-model can be seen in Table 5. For the interfaces, steel anchor and cementitious grout, the previously presented properties were used (Section 3.2). The bricks and the mortar were defined as nonlinear materials using the constitutive model described in the previous sections (exponential softening for the tensile part, and a parabolic behaviour in compression). All the material properties were

set according to their experimental evaluation (Muñoz et al, 2019; Muñoz and Lourenço, 2019).

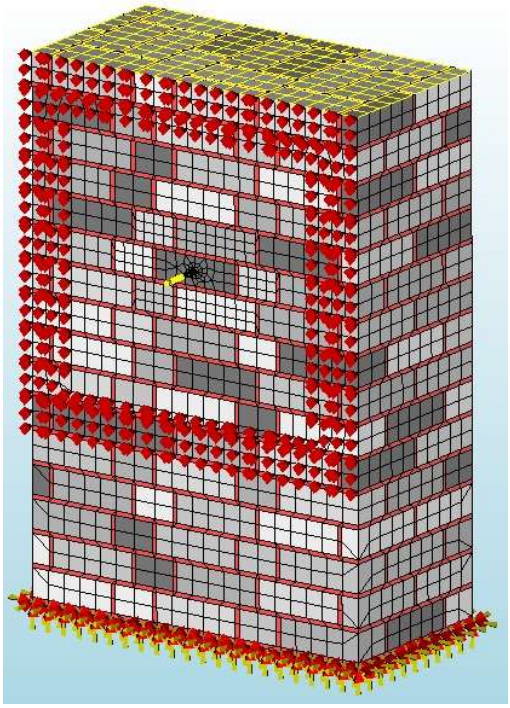

*Figure 21 – Brick wall FE mesh for the micro-model*

*Table 5 – Mechanical properties for the micro-model*

| Property | Brick unit | Mortar |
|---|---|---|
| Young's modulus, $E$ (GPa) | 9.74 | 2.15 |
| Compressive strength, $f_c$ (MPa) | 19.90 | 1.42 |
| Fracture energy in compression, $G_c$ (N/mm) | 22.13 | 2.30 |
| Tensile strength, $f_t$ (MPa) | 2.13 | 0.41 |
| Mode-I Fracture energy, $G_f$ (N/mm) | 0.01 | 0.01 |

The results obtained, in terms of force – displacement curve can be seen in Figure 22a. The maximum capacity is overestimated by the numerical model in 23%, when comparing to the experimental results. Here, the maximum capacity obtained is 26.9 kN (20.78 kN for experimental). Considering that the mechanical parameters used in this model came directly from experimental characterization and no changes were made to the values, as well as the fact that the experimental curve represents only one wall, , the obtained results could be considered reasonable. It should also be highlighted that this

model is able to reproduce the damage evolution and in particular the final crack pattern (Figure 22b).

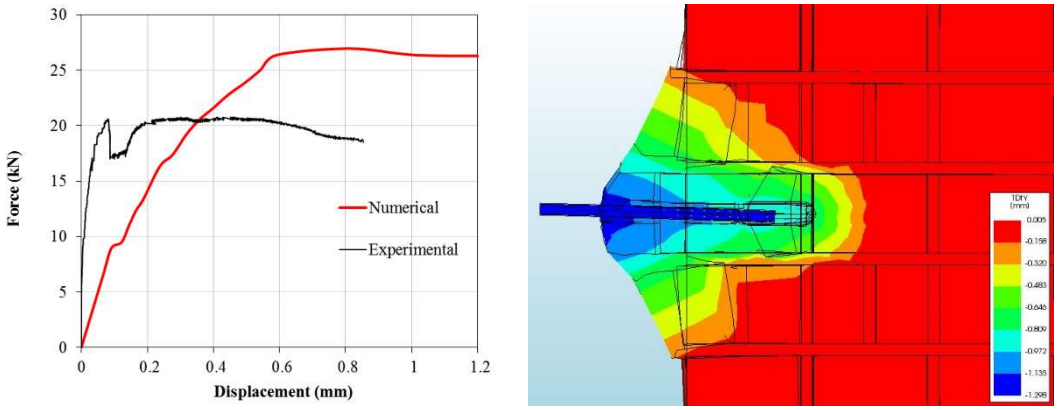


*Figure 22 – Micro-model results: a) force-displacement curve; b) cone failure.*

## 4. Conclusions

This work presents a numerical study of the behaviour of masonry walls and grouted anchoring systems, aiming at providing recommendations on adequacy of modelling approaches. It seems clear that numerical analyses are capable of prediction the behaviour of this systems in terms of ultimate capacity, nonlinear behaviour and failure mechanisms, but special care is required because the size of the masonry units influence the results. This work can also be used in the pursuit of future parametric studies.

All the developed numerical models were compared with the experimental data. The macro pull-out model has given good results for what concern the cone breakout masonry failure and the mechanisms of damage evolution. Here, the masonry was modelled as an isotropic homogeneous material where the nonlinear behaviour was introduced by a constitutive law using rotating crack model, considering exponential softening in tension and parabolic behaviour in compression. The steel bar and the grout were assumed as linear elastic materials, coherent with the experimental damage observed. The results

found using the material properties for masonry arising from the diagonal compression models have been excessively conservative, in particular for what concern the stone masonry. However, it was shown that with some additional considerations to the mechanical properties involving the geometry and properties of the masonry constituents, it should be possible to estimate the maximum capacity of these anchors systems.

The influence of the geometry of the unit where the anchor is applied was highlighted. This phenomenon has a lower impact for the brick masonry, as it is constituted by smaller units arranged in a more precise and repetitive way. The random dispositions of the stone units, their arrangement in the wall, their shape and geometry have high influence on the final results as regards to loadbearing capacity, breakout cone dimensions and total displacements, for the stone wall. This is related to the dimension of the anchoring system itself, since it could be considered as a short anchor. Nevertheless, the unit model, in which the anchored unit is considered linear elastic, was able to improve the results, when compared with the initial macro-model, namely for the stone masonry. This model could be an alternative when dealing with masonry composed of large units.

The micro-model turned out to be the model which resulted in the lower difference when compared with the experimental results, considering directly the mechanical properties obtained from experimental tests. The model has slightly overestimated the capacity of the grouted anchor and the approach has some drawbacks. Compared to the other modelling approaches, it requires a more complex definition of the mechanical model and considerably more computational effort.

The results presented in this study should be taken with caution, as the experimental study on which it is based is composed of only one specimen of each type of masonry. Nevertheless, the anchoring system has been modelled numerically using different

approaches and it was made clear that modelling this type of system has several challenges. Because a local failure mechanism, associated to a single unit, is found rather than a global one, using average mechanical properties from masonry tests does not seem to be a reasonable option, leading to a clear underestimation of the anchor capacity. This can be overcome with considerations, which are dependent on the system itself (both anchor and type of masonry wall). The unit model presented here helps in minimizing this effect and may be used when an expedite estimation of the anchor capacity is needed, still conservatively. The micro-modelling approach seems to be the most accurate one, however it requires the most resources and a detailed knowledge of the geometry of masonry walls, which often is not available.

## 5. References

Abruzzese D, Miccoli L, Vari A (2009) *Dynamic investigations on medieval masonry towers: vibration measurements and structural identification*. Proceedings of the Protection of Historical Buildings – Prohitech 09, pp. 807-813.

Annecchiarico M, Portioli F, Landolfo R (2009) *FE simulation of masonry wall samples of Mustafa Pasha mosque by homogeneous continuum models: analysis and calibration*. Proceedings of the Protection of Historical Buildings – Prohitech 09, pp. 95-100.

Araújo A (2014) *Modelling of the Seismic Performance.* PhD thesis. Guimarães: Universidade do Minho.

Aşıkoğlu A, Vasconcelos G, Lourenço PB, Pantò B (2020) *Pushover analysis of unreinforced irregular masonry buildings: Lessons from different modeling approaches*. Engineering Structures 218, 110830.

Banholzer B, Brameshuber W, Jung W (2005) *Analytical simulation of pull-out tests-the direct problem*. Cement e Concrete Composites 27(1), pp. 93-101.

Benmokrane B, Zhang B, Chennouf A (2000) *Tensile properties and pullout behaviour of AFRP and CFRP rods for grouted anchor applications*. Construction and Building Materials 14(3), pp. 157-170.

Berto L, Saetta A, Scotta R, Vitaliani R (2004) *Shear behaviour of masonry panel: parametric FE analysis*. International Journal of Solids and Structures 41, pp. 4383-4405.

Betti M, Galano L, Vignoli A (2014) *Comparative analysis on the seismic behaviour of unreinforced masonry buildings with flexible diaphragms*. Engineering Structures 61, pp. 195-208.

Betti M, Vignoli A (2008) *Modelling and analysis of a Romanesque Church under earthquake loading: assessment of seismic resistance*. Earthquake Structures 30, pp. 352-367.

Blondet M, Torrealva D, Vargas J, Velasquez J, Tarque N (2006) *Seismic Reinforcement of Adobe Houses using External Polymer Mesh*. First European Conference on Earthquake Engineering and Seismology, Geneva, Switzerland.

Ciocci MP, Sharma S, Lourenço PB (2018) *Engineering simulations of a super-complex cultural heritage building: Ica Cathedral in Peru*. Meccanica 53, pp. 1931-1958.

Cook RA (2006) *Behavior of Adhesive Bonded Anchors*. American Concrete Istitute Structural Journal 103(6), pp. 822-831.

Dudeka D, Kadela M (2016) *Pull-Out Strength of Resin Anchors in Non-cracked and Cracked Concrete and Masonry Substrates*. Procedia Engineering 161, pp. 864-867.

Gigla B (2004) Bond *strength of infection anchors as suplementary reinforcement inside historic masonry*. Proceedings of the 13th International Brick and Block Masonry Conference, Amsterdam, Netherlands.

Lourenço PB (1996) *Computational strategies for masonry structures*. PhD thesis. Delft University of Technology.

Lourenço PB (2002) *Computations on historic masonry structures*. Progress in Structural Engineering and Materials 4, pp. 301-319.

Lourenço PB (2009) *Recent advances in masonry modelling: micromodelling and homogenization*. Multiscale Modelling in Solid Mechanics, pp. 251-294.

Lourenço PB, Ciocci MP, Greco F, Karanikoloudis G, Cancino C, Torrealva D, Wong K (2018) *Traditional Techniques for the Rehabilitation and Protection of Historic Earthen Structures: The Seismic Retrofitting Project*. International Journal of Architectural Heritage 13:1, pp. 15-32.

Lourenço PB, Mendes N, Ramos LF, Oliveira DV (2011). *On the analysis of masonry structures without box behavior*. International Journal of Architectural Heritage 5, pp. 369-382.

Manie J, Kikstra WP (2016) *DIANA Finite Element Analysis,User's Manual release 10.0-Material Library.* Delft: TNO DIANA

Moreira S, Ramos L, Oliveira D, Lourenço PB (2014) *Experimental behavior of masonry wall-to-timber elements connections strengthened with injection anchors*. Engineering Structures 81, pp. 98-109.

Muñoz R, Lourenço PB (2019) *Mechanical Behaviour of Metal Anchors in Historic Brick Masonry: An Experimental Approach.* Structural Analysis of Historical Constructions. RILEM Bookseries, vol 18. Springer, pp. 788-798.

Muñoz R, Lourenço PB, Moreira S (2019) *Experimental results on mechanical behaviour of metal anchors in historic stone masonry.* Construction and Building Materials 163, pp. 643-655.

NTC (2018) *Norme tecniche per le costruzioni. With Circolare from January 21, no. 7 (2019) from Ministry of infrastructure and transportation*. Italy (in Italian).

Pereira JM, Correia A, Lourenço PB (2020) *In-plane behaviour of rubble stone masonry walls: experimental, numerical and analytical approach*. Construction and Building Materials, 121548.

Scotta R, Trulalli D, Marchi L, Pozza L (2018) Seismic performance of URM buildings with in-plane non-stiffened and stiffened timber floors. Engineering Structures 167, pp. 683-694.

Tolles EL, Webster FA, Crosby A, Kimbro EE (1996) *Survey of Damage to Historic Adobe Buildings after the January 1994 Northridge Earthquake*. Getty Conservation Institute, Los Angeles, US.

Tomazevic M (1999) *Earthquake-resistant design of masonry buildings*. Imperial College Press.

Torrealva D (2012) *Seismic Design Criteria for Adobe Buildings Reinforced with Geogrids*. In: Proceedings of the 15th World Conference on Earthquake Engineering, Lisbon, Portugal.

Torrealva D, Vicente EF (2014) *Experimental behaviour of traditional seismic retrofitting techniques in earthen buildings in Peru*. Proceedings of the 9th International Conference on Structural Analysis of Historical Constructions, SAHC 2014, Mexico City, Mexico.

Varum H, Tarque N, Silveira D, Camata G, Lobo B, Blondet M, Figueiredo A, Rafi MM, Oliveira C, Costa A (2014) *Structural Rehabilitation of Old Buildings, Building Pathology and Rehabilitation 2*, Springer-Verlag, Berlin Heidelberg.

Wang D, Wu D, Ouyang C, He A, Sun X (2017) *Simulation analysis of large-diameter post-installed anchors in concrete*. Construction and Building Materials 143, pp. 558-565.